Available online at www.sciencedirect.com
ScienceDirect
Trans. Nonferrous Met. Soc. China 27(2017) 2434−2442
Transactions of Nonferrous Metals Society of China
www.tnmsc.cn

Modeling of deformation energy at elevated temperatures and its application in Mg−Li−Al−Y alloy

Fu-rong CAO[1], Bi-jin ZHOU[1,2], Bin YIN[1,3], Guo-qiang XUE[1,4], Xiao-tong ZHU[1,5], Guang-ming XU[6]

1. School of Materials Science and Engineering, Northeastern University, Shenyang 110819, China;
2. School of Materials Science and Engineering, Shanghai Jiao Tong University, Shanghai 200240, China;
3. Wuhu Cowin Automobile Co., Ltd., Wuhu 241000, China;
4. Xi'an Supercrystal Science and Technology Development Co., Ltd., Xi'an 710016, China;
5. Huai'an Dekema Semiconductor Co., Ltd., Huai'an 223300, China;
6. Key Laboratory of Electromagnetic Processing of Materials, Ministry of Education, Northeastern University, Shenyang 110819, China

Received 1 July 2016; accepted 4 January 2017

Abstract: To control the superplastic flow and fracture and examine the variation in deformation energy, the stress and grain size of Mg−7.28Li−2.19Al−0.091Y alloy were obtained using tensile testing and microstructure quantification, and new high temperature deformation energy models were established. Results show that the grain interior deformation energy increases with increasing the strain rate and decreases with increasing the temperature. The variation in the grain boundary deformation energy is opposite to that in the grain interior deformation energy. At a given temperature, critical cavity nucleation energy decreases with increasing strain rate and cavity nucleation becomes easy, whereas at a given strain rate, critical cavity nucleation energy increases with increasing temperature and cavity nucleation becomes difficult. The newly established models of the critical cavity nucleation radius and energy provide a way for predicting the initiation of microcrack and improving the service life of the forming parts.
Key words: high temperature deformation; superplasticity; creep; deformation energy; Mg−Li−Al−Y alloy

1 Introduction

High temperature deformations such as superplasticity and creep have attracted the attention of researchers in the past [1,2], and limited energy analyses have been recorded. GITTUS [3] obtained the theoretical free energy for superplasticity and creep and applied them in zircaloy. He believed that high ductility of superplastic materials is due to the low free energy. VALIEV et al [4] and GERTSMAN et al [5] proposed the models of energy of non-equilibrium grain boundary and provided a basis for elucidating grain boundary behavior during deformation. Recently, GALINDO-NAVA et al [6] employed thermodynamics to investigate the cavitation effects and obtained the cavity growth equation. They also obtained the optimal conditions for superplastic behaviour. However, the parameters K and K' in the constitutive equation in Gittus's energy model cannot be determined in other materials and owing to the restriction of research history, the estimation of the number of dislocations at grain boundary in some models [4,5] was treated as number instead of a model. Therefore, it is necessary to connect available model of number of dislocations at grain boundary to their models of non-equilibrium grain boundary energy. In the meantime, efforts are made to establish new high temperature deformation energy models. Except that the model of grain boundary deformation energy is modified on Russian researchers' work, other models such as macroscopic deformation energy, grain interior deformation energy and cavity nucleation (microcrack initiation) deformation energy are all newly established for superplastic flow and fracture process. The scientific value of the cavity nucleation energy model is to control microcrack initiation, avoid the premature fracture of forming part and improve the service life of forming part.

Foundation item: Project (51334006) supported by the National Natural Science Foundation of China
Corresponding author: Fu-rong CAO; Tel: +86-24-83670183; E-mail: cfr-lff@163.com
DOI: 10.1016/S1003-6326(17)60270-X

Because of the extremely low density, high specific strength and high specific stiffness, good damping properties and electromagnetic shielding property, Mg−Li alloys have the potential for use in areas such as spaceflight, weapons, 3C products and automobile manufacturing and have received extensive attention in recent years [7−9]. JIANG et al [10] reported the effect of Sn addition on the microstructures of Mg−5Li alloys and found that Sn addition has a strong grain refinement effect on Mg−5Li alloy. YAN et al [11] investigated the microstructures and mechanical properties of cold-rolled Mg−8Li and Mg−8Li−2Al−2RE alloys and found that Mg−8Li−2Al−2RE alloy had the yield strength of 187 MPa with an elongation of 21%. KONG et al [12] investigated the microstructure and mechanical properties of two-phase Mg−10.73Li−4.49Al−0.52Y alloy processed by ECAP and obtained the tensile strength of 166.4 MPa. However, to the best of our knowledge, little information is available on the high temperature energy model in Mg−Li alloy. It is necessary, therefore, to investigate the variation in deformation energy and to obtain the distribution of deformation energy at elevated temperatures under different deformation conditions in Mg−Li alloy. We hope that this first report on deformation energy at elevated temperatures in Mg−Li alloy stimulates interests in extensive researchers.

In this work, new high temperature energy models are established. The sheets of a novel Mg−Li−Al−Y alloy are fabricated by casting, rolling and annealing. The stress and grain size at elevated temperatures are determined. The energy models newly derived are calculated in such an alloy.

2 Modeling

2.1 Macroscopic deformation energy

High temperature deformation energy includes macroscopic deformation energy and microscopic deformation energy. The macroscopic deformation energy (macroscopic deformation energy per unit volume) E obeys the following relation:

$$E=\frac{1}{V}\int_{L_0}^{\Delta L_0}F\mathrm{d}S \tag{1}$$

where V is the volume of deformation body, L_0 is the initial gauge length, ΔL_0 is the length increment, F is the external force and S is the displacement of tensile crosshead.

2.2 Grain interior deformation energy

During mechanism research of superplasticity and creep, LANGDON [13] proposed that the grain size is less than the subgrain size in superplasticity and the grain size is greater than the subgrain size in dislocation creep.

For superplasticity, the microscopic deformation energy is dissipated into grain interior deformation energy, grain boundary deformation energy, cavity nucleation energy and so forth. Presuming that dislocations move across a grain in length L under applied stress and the grain size L is less than the subgrain size λ [13] and that the dislocation slip distance is equal to the grain size L and the dislocation line length is equal to the grain size L, the grain interior deformation energy (deformation energy per unit area of a grain interior) E_{IS} obeys the following relation:

$$E_{\mathrm{IS}}=\frac{N_{\mathrm{IS}}\dfrac{\sigma}{\sqrt{3}}bLL}{\dfrac{\pi}{4}L^2}=\frac{4}{\pi}\left(N_{\mathrm{IS}}\frac{\sigma}{\sqrt{3}}b\right) \tag{2}$$

where b is the magnitude of Burgers vector of dislocation, L is the linear intercept grain size and N_{IS} is the number of dislocations inside a grain [14].

$$N_{\mathrm{IS}}=\frac{(1-\nu)L\pi\sigma}{\sqrt{3}Gb} \tag{3}$$

where v is the Poisson ratio and G is the shear modulus.

Substituting Eq. (3) into Eq. (2) gives

$$E_{\mathrm{IS}}=\frac{4}{3}(1-\nu)\left(\frac{\sigma}{G}\right)\sigma L \tag{4}$$

For dislocation creep, subgrains may exist in a grain. The microscopic deformation energy is dissipated into grain or subgrain interior deformation energy, grain or subgrain boundary deformation energy, cavity nucleation energy and so forth. Presuming that dislocations move across a subgrain in length λ under applied stress and the dislocation slip distance is roughly equal to the subgrain size $\lambda(=20Gb/\sigma)$ [15] and that the dislocation line length is roughly equal to the subgrain size $\lambda(=20Gb/\sigma)$ [13], the subgrain interior deformation energy (deformation energy per unit area of a subgrain interior) E_{IS} obeys the following relation:

$$E_{\mathrm{IS}}=\frac{N_{\mathrm{IS}}\dfrac{\sigma}{\sqrt{3}}b\lambda\lambda}{\dfrac{\pi}{4}\lambda^2}=\frac{4}{\pi}\left(N_{\mathrm{IS}}\frac{\sigma}{\sqrt{3}}b\right) \tag{5}$$

where N_{IS} is the number of dislocations inside a subgrain.

Similar to the treatment in Eq. (3), one gets

$$N_{\mathrm{IS}}=\frac{(1-\nu)\lambda\pi\sigma}{\sqrt{3}Gb} \tag{6}$$

Substituting Eq. (6) into Eq. (5) gives

$$E_{\mathrm{IS}}=\frac{4}{3}(1-\nu)\left(\frac{\sigma}{G}\right)\sigma\lambda=\frac{80}{3}(1-\nu)\sigma b \tag{7}$$

In addition, for dislocation creep, the grain interior

deformation energy E_{IS} abides by Eq. (4).

2.3 Grain boundary deformation energy

The grain boundary deformation energy (deformation energy per unit area of a grain boundary, $E_{gb}-\gamma$) abides by the following relation [5]:

$$E_{gb}-\gamma=\frac{Gb^2}{4\pi(1-\nu)L'}\cdot\left(\ln\frac{L'}{H}+\frac{1}{N_{gb}}\ln\frac{H}{b}+\frac{4}{N_{gb}}\ln\frac{2L'}{H}+\ln\frac{L'}{H}\ln\frac{H}{b}\right) \quad (8)$$

where E_{gb} is the non-equilibrium grain boundary energy, L' is the grain boundary length in the direction normal to trapped lattice dislocation (TLD) line, 10^3b, H is the width of the complex of TLD dissociation products, N_{gb} is the number of dislocations at grain boundary and γ is the grain boundary surface energy.

The number of dislocations at grain boundary N_{gb} is given by [16]

$$N_{gb}=(1-\nu)\left(\frac{d}{2b}\right)\left(\frac{F'}{Gb}\right) \quad (9)$$

where d is the spatial grain size, $F'=b\sigma\sin\alpha\cdot\cos\alpha$, here $\alpha=30°$. Substituting Eq. (9) into Eq. (8) gives the modified model of grain boundary deformation energy, as

$$E_{gb}-\gamma=\frac{Gb^2}{4\pi(1-\nu)L'}\left(\ln\frac{L'}{H}+\frac{4.62}{(1-\nu)}\left(\frac{b}{d}\right)\left(\frac{G}{\sigma}\right)\ln\frac{H}{b}+\frac{18.5}{(1-\nu)}\left(\frac{b}{d}\right)\left(\frac{G}{\sigma}\right)\ln\frac{2L'}{H}+\ln\frac{L'}{H}\ln\frac{H}{b}\right) \quad (10)$$

In addition, owing to the complexity of subgrain boundary, no approach is found to obtain the number of dislocations and the subgrain boundary deformation energy.

2.4 Cavity nucleation energy

Cavity or cavitation is a common experimental phenomenon in high temperature deformation, especially in superplasticity and dislocation creep. Based on the solid state thermodynamics, the following relation of cavity nucleation energy ΔG in Al−Si−Mg alloy was proposed [17]:

$$\Delta G=-2.53\left(\frac{2}{3}\frac{d}{1.74b}\frac{\sigma^2}{G}\right)r^3+[9.31\gamma-0.5\times2.93\gamma]r^2-3.79\frac{\left(\frac{2}{3}\frac{d}{1.74b}\frac{\sigma^2}{G}\right)^2}{2E}r^3 \quad (11)$$

where d is the spatial grain size, $d=1.74L$, E is elastic modulus, $E=2G(1+\nu)$, and r is the cavity radius .

Here, critical cavity nucleation radius (r_c) is as follows:

$$r_c=40.95\frac{\gamma}{\sigma}\Big/\left\{\left[7.89+2.18\left(\frac{d}{b}\right)\left(\frac{\sigma}{G}\right)\left(\frac{\sigma}{E}\right)\right]\left(\frac{d}{b}\right)\left(\frac{\sigma}{G}\right)\right\} \quad (12)$$

As $\sigma/E\approx0$ is rather small at elevated temperature, Eq. (12) is reduced to Eq. (13):

$$r_c=5.2\left(\frac{\gamma}{\sigma}\right)\left(\frac{b}{d}\right)\left(\frac{G}{\sigma}\right) \quad (13)$$

Substituting Eq. (13) into Eq. (11) gives critical cavity nucleation energy, usually $\gamma=1$ J/m^2.

$$\Delta G_c=76\left(\frac{b}{d}\right)^2\left(\frac{G}{\sigma}\right)^2\left(\frac{1}{\sigma}\right)^2 \quad (14)$$

Shear modulus G for magnesium can be written as [18]

$$G=1.66\times10^4\left[1-0.49\left(\frac{T-300}{924}\right)\right] \quad (15)$$

For high temperature deformation of Mg−7.28Li−2.19Al−0.091Y alloy investigated here, the grain size d and the true stress σ can be expressed as follows based on the Zener−Hollomon parameter (Z)[19−23]:

$$d=cZ^{-q}=57.34Z^{-0.043} \quad (16)$$

$$\sigma=23.256\sinh^{-1}\left[Z/\exp17.111\right]^{0.517} \quad (17)$$

$$Z=\dot{\varepsilon}\exp[Q/(RT)]=\dot{\varepsilon}\exp[111290/(8.134T)] \quad (18)$$

where Q is the activation energy for deformation and R is the mole gas constant.

Substituting Eqs. (15)−(18) into Eq. (13) gives

$$r_c=8.93\times10^{-10}\left[1-0.49\left(\frac{T-300}{924}\right)\right]\cdot\left[\dot{\varepsilon}\exp(111290/8.314T)\right]^{0.043}\cdot\left\{\sinh^{-1}\left[\dot{\varepsilon}\exp(111290/8.314T)/\exp17.111\right]^{0.517}\right\}^{-2} \quad (19)$$

Substituting Eqs. (15)−(18) into Eq. (14) gives

$$\Delta G_c=2.24\times10^{-18}\left[\dot{\varepsilon}\exp(111290/8.314T)\right]^{0.086}\cdot\left\{\frac{1-0.49\left(\frac{T-300}{924}\right)}{\sinh^{-1}\left[\dot{\varepsilon}\exp(111290/8.314T)/\mathrm{e}17.111\right]^{0.517}}\right\}^2\cdot\left\{\sinh^{-1}\left[\dot{\varepsilon}\exp(111290/8.314T)/\exp17.111\right]^{0.517}\right\}^{-2} \quad (20)$$

Equations (19) and (20) reveal that critical cavity nucleation radius r_c and energy ΔG_c can be calculated according to the deformation conditions such as temperature and strain rate.

3 Experimental

A Mg−7.28Li−2.19Al−0.091Y alloy was prepared by melting pure Mg, pure Li and Al−30%Y master alloy covered with 75%LiCl+25%LiF flux under the protection of argon in an electric resistance furnace. The melt was cast at the temperature of 983 K into rectangular ingots in a copper mould cooled by circulating water. When being homogenized at the temperature of 473 K for 20 h, the ingots were hot rolled with a reduction of 77.3% and cold rolled into sheets of 2 mm in thickness with a reduction of 60%. Dogbone samples whose direction is parallel to the longitudinal rolling direction were made on a stamping machine. The dimensions of the dogbone samples were 10 mm in gauge length, 6 mm in width and 2 mm in thickness. The samples were annealed at the temperature of 623 K for 2 h. Tensile tests were conducted at temperatures ranging from 473 to 623 K over strain rates ranging from 1.67×10^{-2} to 1.67×10^{-4} s^{-1} on SANS CMT5105 universal tensile machine. The samples for optical microscope (OM) observation were ground, polished and etched in a solution of 10% HCl + 90% EtOH. OM microstructures were observed by OLYMPUS 500 microscope. The linear intercept grain sizes were measured by Image Pro Plus software.

To calculate the deformation energy, physical parameters are presented in Table 1 [24,25].

Table 1 Physical parameters of Mg [24, 25]

V/mm^3	$b/10^{-10}$m	ν	γ/(J·m^{-2})	$L'/10^{-7}$ m
120	3.21	0.28	1.0	3.21

4 Results and discussion

4.1 Macroscopic deformation energy

The load−displacement curves at different temperatures ranging from 473 to 623 K with strain rates ranging from 1.67×10^{-4} to 1.67×10^{-2} s^{-1} are shown in Fig. 1. The deformation temperature and strain rate have a considerable effect on the deformation load. The load decreases as the temperature increases and/or the strain rate decreases. The maximum elongation to failure of 265.8% (S/L_0=26.58/10) appears at 623 K with an initial strain rate of 5×10^{-4} s^{-1}, manifesting that the present alloy exhibits quasi-superplasticity or superplasticity-like behavior.

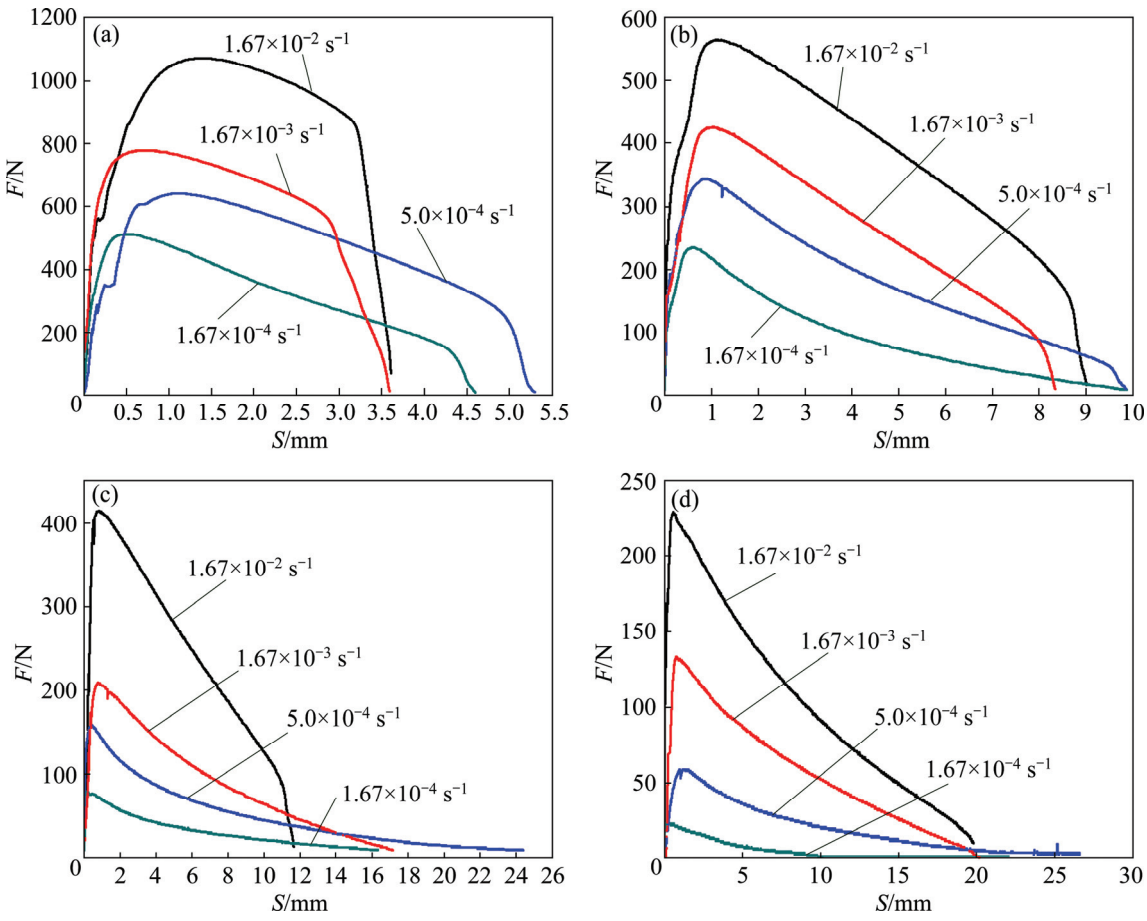

Fig. 1 Load−displacement curves at different strain rates and temperatures: (a) 473 K; (b) 523 K; (c) 573 K; (d) 623 K

As shown in Eq. (1), at a given displacement, the higher the stress or the strength of the alloy, the higher the macroscopic deformation energy. In this case, macroscopic energy reflects the magnitude of the stress or the strength to a certain extent. Because total deformation energy is composed of strain energy and interfacial energy in the alloy, macroscopic deformation energy is dissipated into such energy and is a measure of the capability of the alloy in resisting deformation.

Macroscopic deformation energy as a function of temperature and strain rate is shown in Fig. 2. The deformation temperature and strain rate have remarkable effects on the macroscopic deformation energy. The higher the temperature and/or the lower the strain rate, the lower the macroscopic deformation energy. When the temperature is constant, the macroscopic deformation energy decreases with decreasing the strain rate. When the strain rate is constant, the macroscopic deformation energy decreases with increasing the temperature. The reason is that lower strain rate and/or higher temperature accelerates the thermal activation process, speeds up atomic diffusion and causes the dislocations in the deformation body to slide easily.

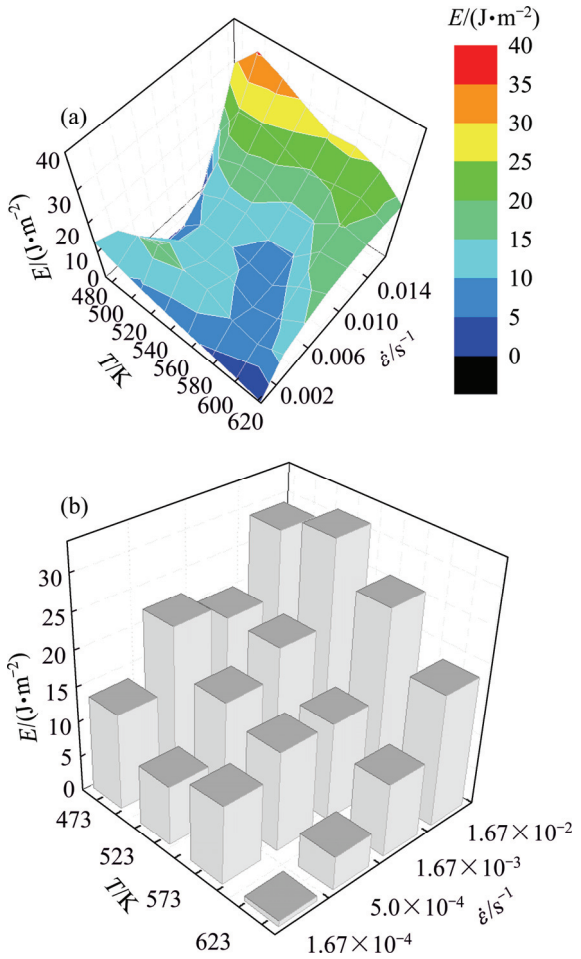

Fig. 2 Macroscopic deformation energy as function of temperature and strain rate: (a) E–T–$\dot{\varepsilon}$ diagram; (b) E–T–$\dot{\varepsilon}$ histogram

4.2 Grain interior deformation energy

The fracture stresses of fracture samples are shown in Table 2. The stress means true stress. The linear intercept grain sizes of fracture samples are shown in Table 3. Because it is difficult to determine the subgrain size λ in the present alloy by transmission electron microscope, the determination of the subgrain interior deformation energy using Eq. (7) is omitted. Substituting the Poisson ratio in Table 1, the fracture stresses in Table 2 and the linear intercept grain sizes in Table 3 into Eq. (4) gives the grain interior deformation energy at fracture strain. Figure 3 shows the grain interior deformation energy as a function of strain rate and temperature.

Table 2 Fracture stress of Mg−7.28Li−2.19Al−0.091Y fracture sample

T/K	σ/MPa			
	1.67×10^{-2} s^{-1}	1.67×10^{-3} s^{-1}	5×10^{-4} s^{-1}	1.67×10^{-4} s^{-1}
473	95.57	52.34	34.02	20.07
523	34.98	18.43	8.84	2.65
573	19.90	9.92	5.30	2.40
623	10.66	5.55	2.01	1.36

Table 3 Linear intercept grain size of Mg−7.28Li−2.19Al−0.091Y fracture sample

T/K	L/μm			
	1.67×10^{-2} s^{-1}	1.67×10^{-3} s^{-1}	5×10^{-4} s^{-1}	1.67×10^{-4} s^{-1}
473	15.92	16.75	17.2	17.84
523	13.74	14.2	14.95	15.31
573	23.19	19.8	18.22	19.2
623	21.53	25.36	20.56	22.46

It is found in Fig. 3(a) that at the temperature of 473 K, the grain interior deformation energy increases sharply with increasing the strain rate and is higher, whereas at temperatures ranging from 523 to 623 K, the grain interior deformation energy increases slightly with increasing the strain rate and is lower, much lower than that at the temperature of 473 K.

It is found in Fig. 3(b) that at the given strain rate of 1.67×10^{-2} s^{-1}, the grain interior deformation energy decreases sharply with increasing the temperature and is higher, whereas at the constant strain rates ranging from 1.67×10^{-3} to 1.67×10^{-4} s^{-1}, the grain interior deformation energy decreases slightly with increasing the temperature, much lower than that at the strain rate of 1.67×10^{-2} s^{-1}.

Compared with the effect of strain rate on the grain interior deformation energy, the effect of temperature on the grain interior deformation energy is more significant. The reason is that as the temperature increases and the strain rate decreases, the degree of strain hardening

decreases, vacancy concentration inside the grain increases and lattice diffusion accelerates. All of these lead to easier dislocation slip and climb, and decrease in number of dislocations inside the grain. Therefore, the grain interior deformation energy decreases much obviously with the increase in the deformation temperature.

4.3 Grain boundary deformation energy

Substituting the data in Tables 1−3 into Eq. (10) gives the grain boundary deformation energy at fracture strain. Figure 4 shows the grain boundary deformation energy as a function of H/L' ratio at different strain rates at different temperatures. At a constant temperature, the lower the strain rate, the higher the grain boundary deformation energy, while at a constant strain rate, the higher the temperature, the higher the grain boundary deformation energy. Abnormal situation appears at the temperature of 573 K.

Variation in the grain interior deformation energy is opposite to the variation in the grain boundary deformation energy. It is suggested that dislocations

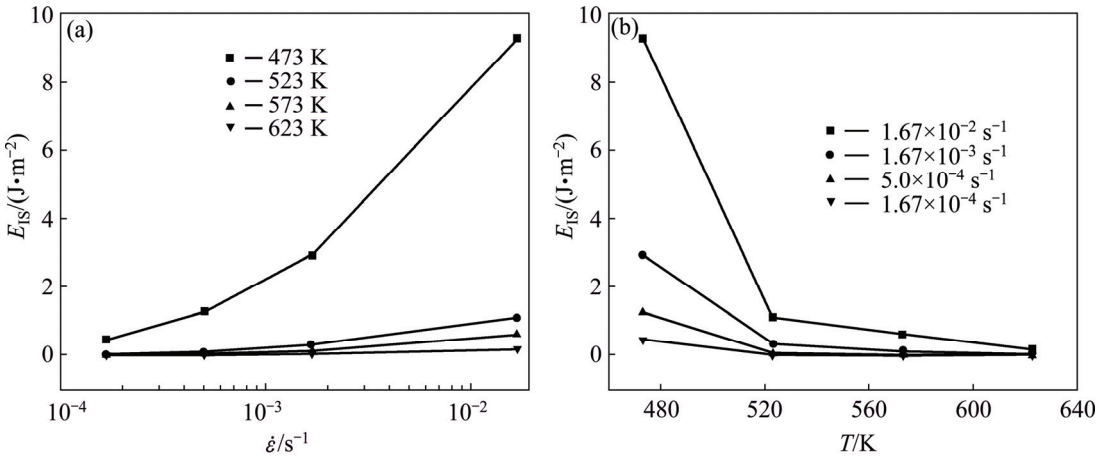

Fig. 3 Grain interior deformation energy versus strain rate (a) and temperature (b)

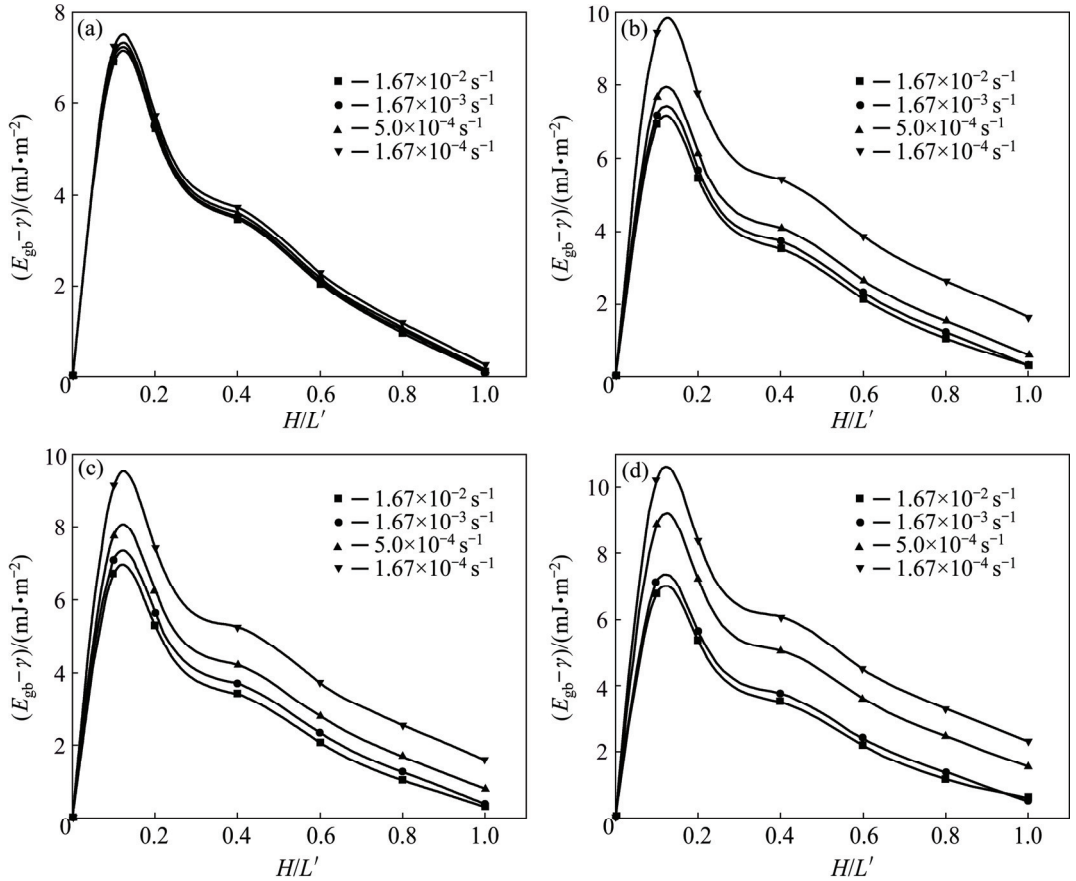

Fig. 4 Grain boundary deformation energy as function of H/L ratio at different strain rates and different deformation temperatures: (a) 473 K; (b) 523 K; (c) 573 K; (d) 623 K

inside the grain are trapped by the grain boundary via dislocation slip and climb, which results in the reduction of lattice defects and the increase in grain boundary defects. For this reason, the grain interior deformation energy decreases and the grain boundary deformation energy increases as the temperature increases and the strain rate decreases.

4.4 Critical cavity nucleation energy

Because cavity nucleation often takes place in the early stage of deformation at elevated temperatures, researchers usually choose the strain ranging from 0.1 to 0.3. Here, the strain of 0.2 is used. The stresses of Mg−7.28Li−2.19Al−0.091Y alloy at a true strain of 0.2 are shown in Table 4. The stress values were substituted into Eq. (14) and the critical cavity nucleation free energy was calculated. The critical cavity nucleation energy as a function of strain rate and temperature is shown in Fig. 5. At a constant temperature, with the increase in strain rate, the stress increases, the critical cavity nucleation radius decreases, and the critical cavity nucleation energy decreases, which indicate that cavity nucleation becomes easy. At a constant strain rate, with the increase in temperature, the stress decreases, the critical cavity nucleation radius increases, and the critical cavity nucleation energy increases, which indicate that cavity nucleation becomes difficult.

Equation (20) shows that critical cavity nucleation energy is a function of strain rate and deformation temperature, which is proved by Fig. 5. In Fig. 5, the effects of strain rate and deformation temperature on the critical cavity nucleation energy show that as the strain rate decreases and the deformation temperature increases, the critical cavity nucleation energy increases. This means that it is difficult for cavity to overcome the energy barrier or energy peak to nucleate. This is because the material has sufficient time to relax stress concentration at lower strain rate and its rapid atomic diffusion easily takes place at higher temperature. For this reason, the cavity nucleation is hindered. This result is corroborated by the experimental facts [26] in superplastic 7475 aluminum alloy and Supral 220 that reducing the strain rate and/or increasing the deformation temperature would reduce cavitation or cavity.

Table 4 Stress of Mg−7.28Li−2.19Al−0.091Y alloy at true strain of 0.2

T/K	σ/MPa			
	1.67×10^{-2} s^{-1}	1.67×10^{-3} s^{-1}	5×10^{-4} s^{-1}	1.67×10^{-4} s^{-1}
473	110.1	73.17	63.17	39.36
523	58.76	41.06	31.50	17.02
573	41.06	20.13	12.58	6.24
623	22.19	13.01	5.84	1.81

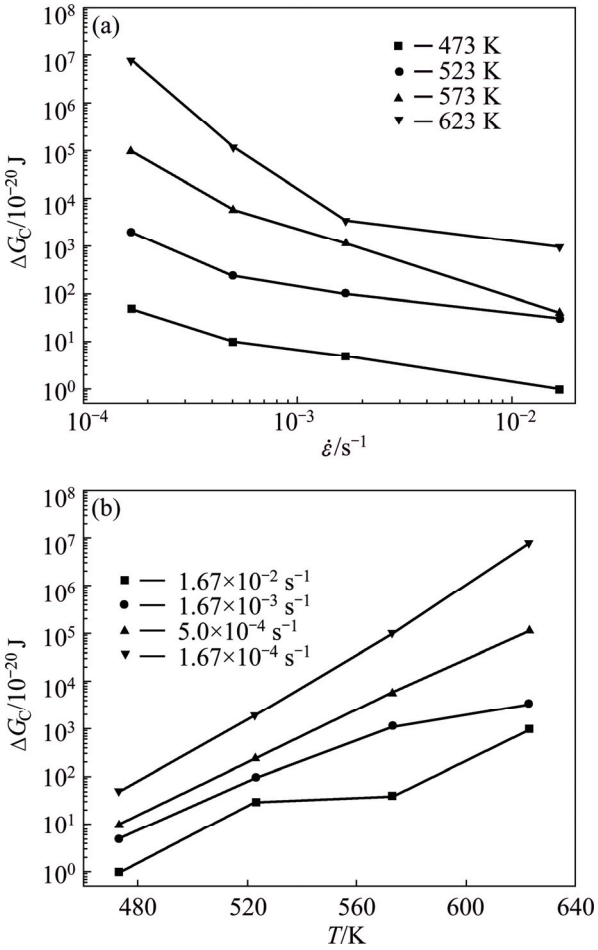

Fig. 5 Critical cavity nucleation energy as function of strain rate (a) and temperature (b)

5 Conclusions

1) The deformation temperature and strain rate have a remarkable effect on the macroscopic deformation energy. The higher the temperature and/or the lower the strain rate, the lower the macroscopic deformation energy.

2) The grain interior deformation energy increases with increasing the strain rate and decreases with increasing the temperature. Compared with the effect of strain rate on the grain interior deformation energy, the effect of temperature on the grain interior deformation energy is more significant.

3) The variation in the grain boundary deformation energy is opposite to the variation in the grain interior deformation energy. At a given temperature, the lower the strain rate, the higher the grain boundary deformation energy, whereas at a given strain rate, the higher the temperature, the higher the grain boundary deformation energy.

4) At a given temperature, critical cavity nucleation energy decreases with increasing strain rate and cavity

nucleation becomes easy, whereas at a given strain rate, critical cavity nucleation energy increases with increasing temperature and cavity nucleation becomes difficult. Critical cavity nucleation radius and energy can be calculated according to the deformation conditions such as temperature and strain rate based on the newly established models.

References

[1] LANGDON T G. Achieving superplasticity in ultrafine-grained metals [J]. Mechanics of Materials, 2013, 67: 2−8.

[2] KASSNER M E, PEREZ-PRADO M T. Five-power-law creep in single phase metals and alloys [J]. Progress in Materials Science, 2000, 45: 1−102.

[3] GITTUS J H. Theoretical free energies for superplasticity and dislocation creep: The origin of the high ductility of superplastic materials [J]. Philosophical Magazine A, 1981, 43: 337−343.

[4] VALIEV R Z, GERTSMAN V Y, KAIBYSHEV O A. Non-equilibrium state and recovery of grain boundary structure: II. Energetic analysis [J]. Physica Status Solidi A, 1983,78: 177−186.

[5] GERTSMAN V Y, VALIEV R Z, KAIBYSHEV O A. On the energy change during the grain boundary structure recovery from non-equilibrium state to equilibrium state [J]. Physica Status Solidi A, 1985, 91: 119−124.

[6] GALINDO-NAVA E I, TORRES-VILLASENOR G, RIVERA-DIAZ-DEL-CASTILLO P E J. Engineering grain boundary sliding and cavitation effects in superplastic alloys employing thermodynamics [J]. Materials Science and Technology, 2015, 31: 677−687.

[7] KIM Yong-Ho, SON Hyeon-Taek. Effects of Li addition on microstructure and mechanical properties of Mg−6Al−2Sn−0.4Mn alloys [J]. Transactions of Nonferrous Metals Society of China, 2016, 26: 697−703.

[8] WEI Guo-bing, PENG Xiao-dong, HU Fa-ping, HADADZADEH A, YANG Yan, XIE Wei-dong, WELLS M A. Deformation behavior and constitutive model for dual-phase Mg−Li alloy at elevated temperatures [J]. Transactions of Nonferrous Metals Society of China, 2016, 26: 508−518.

[9] WU Li-bin, LIU Xu-he, WU Rui-zhi, CUI Chong-liang, ZHANG Jing-huai, ZHANG Mi-lin. Microstructure and tensile properties of Mg−Li−Al−Zn based alloys with Ce addition [J]. Transactions of Nonferrous Metals Society of China, 2012, 22: 779−785.

[10] JIANG Bin, YIN Heng-mei, YANG Qing-shan, LI Rui-hong, PAN Fu-sheng. Effect of stannum addition on microstructure of as-cast and as-extruded Mg−5Li alloys [J]. Transactions of Nonferrous Metals Society of China, 2011, 21: 2378−2383.

[11] YAN Hong, CHEN Rong-shi, HAN En-hou. Microstructures and mechanical properties of cold rolled Mg−8Li and Mg−8Li−2Al−2RE alloys [J]. Transactions of Nonferrous Metals Society of China, 2010, 20: s550−s554.

[12] KONG Jing, LIU Qin, KANG Zhi-xin. Microstructure and mechanical properties of two-phase Mg−10.73Li−4.49Al−0.52Y alloy processed by ECAP [J]. The Chinese Journal of Nonferrous Metals, 2012, 22: 2415−2423. (in Chinese)

[13] LANGDON T G. A unified approach to grain boundary sliding in creep and superplasticity [J]. Acta Metallurgica et Materialia, 1994, 42: 2437−2443.

[14] WATANABE H, MUKAI T, HIGASHI K. Deformation mechanism of fine-grained superplasticity in metallic materials expected from the phenomenological constitutive equation [J]. Materials Transactions, 2004, 45: 2497−2502.

[15] OUYANG D L, FU M W, LU S Q. Study on the dynamic recrystallization behavior of Ti-alloy Ti−10V−2Fe−3V in β processing via experiment and simulation [J]. Materials Science and Engineering A, 2014, 619: 26−34.

[16] PAIDAR V, TAKEUCHI S. Superplastic deformation carried by grain boundaries [J]. Acta Metallurgica et Materialia, 1992, 40: 1773−1782.

[17] CAO F R, LI Z L , ZHANG N X, DING H, YU F X, ZUO L. Superplasticity, flow and fracture mechanism in an Al−12.7Si−0.7Mg alloy [J]. Materials Science and Engineering A, 2013, 571: 167−183.

[18] KAWASAKI M, KUBOTA K, HIGASHI K, LANGDON T G. Flow and cavitation in a quasi-superplastic two-phase magnesium–lithium alloy [J]. Materials Science and Engineering A, 2006, 429: 334−340.

[19] XU T, HU L X, SUN Y. Deformation behaviour and dynamic recrystallization of AZ61 magnesium alloy [J]. Journal of Alloys and Compounds, 2013, 580: 262−269.

[20] LV B J, PENG J, SHI D W, TANG A T, PAN F S. Constitutive modeling of dynamic recrystallization kinetics and processing maps of Mg−2.0Zn−0.3Zr alloy based on true stress–strain curves [J]. Materials Science and Engineering A, 2013, 560: 727−733.

[21] JI G L, LI Q, LI L. The kinetics of dynamic recrystallization of Cu−0.4Mg alloy [J]. Materials Science and Engineering A, 2013, 586: 197−203.

[22] LIU Y G, LI M Q, LUO J. The modelling of dynamic recrystallization in the isothermal compression of 300M steel [J]. Materials Science and Engineering A, 2013, 574: 1−8.

[23] ZHOU Bi-jin. Research on the superplasticity of magnesium−lithium alloy [D]. Shenyang: Northeastern University, 2015. (in Chinese)

[24] FRIEDEL J. Dislocations [M]. Oxford: Pergamon Press, 1964.

[25] CHOKSHI A H. Cavity nucleation and growth in superplasticity [J]. Materials Science and Engineering A, 2005, 410−411: 95−99.

[26] PILLING J, RIDLEY N. Superplasticity in crystalline solids [M]. London, UK: The Institute of Metals, 1989.

高温变形能建模及其在 Mg−Li−Al−Y 合金中的应用

曹富荣[1]，周碧晋[1,2]，尹 斌[1,3]，薛国强[1,4]，朱晓彤[1,5]，许光明[6]

1. 东北大学 材料科学与工程学院，沈阳 110819；
2. 上海交通大学 材料科学与工程学院，上海 200240；
3. 芜湖凯翼汽车有限公司，芜湖 241000；
4. 西安超晶科技发展有限责任公司，西安 710016；
5. 淮安德科码半导体有限公司，淮安 223300；
6. 东北大学 材料电磁过程研究教育部重点实验室，沈阳 110819

摘 要：为了控制超塑性流动和断裂并研究变形能的变化，采用拉伸实验和显微组织定量方法获得 Mg−7.28Li−2.19Al−0.091Y 合金的应力和晶粒尺寸并建立新的高温变形能模型。结果表明，晶粒内部变形能随应变速率增大而增大，随温度升高而降低；晶界变形能的变化与晶粒内部变形能的变化相反。在给定温度下，临界空洞形核能随应变速率增大而降低，使空洞形核变得容易；在给定应变速率下，临界空洞形核能随变形温度升高而增大，导致空洞形核变得困难。新建立的临界空洞形核半径和能量模型为预测微裂纹的产生和提高成形零件的使用寿命提供了一个新途径。

关键词：高温变形；超塑性；蠕变；变形能；Mg−Li−Al−Y 合金

(Edited by Xiang-qun LI)